VNU Journal of Science: Mathematics - Physics

Journal homepage: https://js.vnu.edu.vn/MaP

Original Article

Structural Properties of Liquid $CaO–SiO_2–P_2O_5$ System

Nguyen Mai Anh*, Nguyen Van Hong

Hanoi University of Science and Technology, 1 Dai Co Viet, Hai Ba Trung, Hanoi, Vietnam

Received 30 June 2022
Revised 07 March 2023; Accepted 22 May 2023

Abstract: Crystalline structure of CaO-P_2O_5-SiO_2 system at 3,000 K were investigated by molecular dynamic simulation. The models with different concentrations of P_2O_5 (5-40 mol%) were constructed by using Born-Mayer-Huggins potentials. The size of models was from 5,270-5,520 atoms. The local environment of elements and glassy-network structure were investigated in detail. The radial distribution functions (RDFs) showed that the average first nearest neighbor distances for Ca-O, P-O and Si-O were of 2.28-2.3Å, 1.56-1.58Å and 1.64-1.68Å, respectively. The BO fraction increases and NBO ratio decreases with the uptrend of the concentration of P_2O_5. The change of P_2O_5 content also changes the structures of [SiO4] and [PO4] tetrahedrons clusters.

Keywords: Molecular dynamics simulation, cluster, bridge-bridge bond, coordination number.

1. Introduction

The bioglass was found by Larry Hench in a project of US Army Medical R&D Command in 1969. They desired to have a material that could replace the diseased and damaged bone tissues but not be rejected by the body. The bone contains hydroapatite (HA- $Ca_5(PO_4)_3(OH)$), so the material should be formed in the HA layer in vivo. Therefore, Hench et al., [1, 2] discovered the first bioactive glass-45S5, containing two oxides P_2O_5 and CaO, providing the HA composition and two elements abundant in the human body (SiO_2 and NaO). Nowaday, there are more than 30 elements doped in bioactive glass, so it is important to understand their effects on the structure and properties of bioglass [3]. There are many researches on the properties of the materials in dependence on temperature, pressure [4] and elemental composition ratio [5, 6], etc,…

Ca- and P-based bioglasses were designed and manufactured for biomaterials [7]. Concentrations of Ca^+ and $[PO_4]^-$ in the bodystream are relatively large (namely 1–5 mM) [8]. P_2O_5 is an important compound for determining the property of bioglass in biomedical [9]. Increasing phosphate concentration in gel-glass composition enhances the crystalline phosphate structure, amorphous silicate

* Corresponding author.
E-mail address: Anh.NM212446M@sis.hust.edu.vn

https//doi.org/10.25073/2588-1124/vnumap.4760

(Si-O-Si) and the quantity of bringing oxygen (BO) in SiO_4 tetrahedrons. The pores in the structure and the bioactivity property were also decreased [9]. Another study [10] shows that increasing CaO/P_2O_5 ratio made NBO/BO ratio be rised. This results in declining the degree of polymerization between S and P tetrahedra. The increase in the CaO/P_2O_5 ratio is also accompanied by the surge of density and glass transition temperature [11]. The larger CaO/SiO_2 ratio causes the SOS angle to decline, this is due to the interacts of linkage of BO from SOS with Ca^+ ion [12]. In this work, the authors reported that the Si-O coordination number did not change with different ratios of Ca, P and Si.

Investigating the Cao-P_2O_5-SiO_2 (CPS) systems have also been applied in the metallurgical industry. Phosphorus is a harmful element, thus it should be removed in steels used as bone for human. Dicalcium silicate ($2CaO.SiO_2$) and tricalcium phosphate ($3CaO.P_2O_5$) form a solid solution during dephosphorization treatment in the steelmaking process. Therefore, the CPS slag system is significant in the metallurgical process [13]. The studies [13, 14] showed that coordination numbers (CN) of PO_x, SiO_x decrease slightly and CN of CaO_x increases with increasing P_2O_5 volume. There is insignificant change in distances of Si-O and P-O when the P_2O_5/SiO_2 ratio changes.

There are many researches on CPS systems using following techniques: BET (Brunauer–Emmett–Teller) and BJH (Barrett-Joyner-Halenda) method [15], scanning electron microscopy, energy-dispersive X-ray analysis, and infrared spectroscopy studies [16, 17], molecular dynamic simulation (MDS) [13, 14]. In this work, we investigate the structure of CPS systems with different P/S ratio by using MDS method. We research the microstructure elements about RDFs, bond length, angle in the SiO_x and PO_x units, the ratio of types of connections in CPS system and make a comparison with the results of other works. We also present the ratio of types of connections in CPS system material and structure of clusters of SiO_4 and PO_4 tetrahedrons with different P2O5 contents, which has not been clearly mentioned the previous work.

2. Molecular Dynamics Simulation

In the MDS for CaO-P_2O_5-SiO_2 system, we use Born-Mayer-Huggins (BMH) potential function as following:

$$U_{ij}(r) = \frac{q_i q_j}{r_{ij}} + A_{ij} exp\left(-B_{ij} r_{ij}\right) - \frac{C_{ij}}{r_{ij}^6},$$

where, $U_{ij}(r)$ is the interatomic pair potential. $q_i q_j$ are the charge of ions. r_{ij} is the distance between atoms i and j. A_{ij}, B_{ij}, C_{ij} are parameters of BMH potential (Table 1). The first component of the expression is the Coulomb interaction, the second component is the repulsive interaction at short range, and the third component is the attractive Van der Waal interaction.

Table 1. BMH potential for CPS system [13]

i-j	A_{ij}(eV)	B_{ij}(1/Å)	C_{ij}(eV Å^6)
Ca-Ca	329,171.51	6.25	4.34
Ca-Si	26,684.39	6.25	0
Ca-P	164,585.76	12.50	0
Ca-O	718,088.63	6.06	8.67
Si-Si	2163.18	6.25	0
Si-P	1081.59	12.50	0
Si-O	62,817.23	6.06	0
P-P	0	0	0
P-O	1847.66	3.45	0
O-O	1497,594.32	5.88	17.35

The MD simulations are conducted in the isothermal–isobaric (NPT) ensemble. The initial configuration of the system is generated by randomly seeding the atoms in the simulation cubic box, size 53Å. The models include more than 5,000 atoms (5270-5520 atoms). The atomic composition ratio is (40-x)CaO.xP_2O_5.60SiO_2 with x=5, 10, 15, 20, 25, 30, 40. We have seven models corresponding to seven atomic composition ratios. The models are carried out at constant ambient pressure. To eliminate the initial configuration, the models are heated to a temperature of 5,000 K and held at this temperature for 10^5 time steps. The models are then cooled down to 4,500; 4,000; 3,500 K and finally 3,000 K. At 4,500; 4,000; and 3,500 K, the models are recovered in 10^5 time steps. At a temperature of 3,000 K, the models are restored in about 10^6 simulation time steps to equilibrium. The data of the structure CPS systems are saved and calculated.

We investigate short range order (SRO) structure, intermediate range order (IRO) structure, (RDF), cluster distribution of MO_x and OM_y,…

3. Results and Discussion

3.1. Short Range Order (SRO)

We investigate RDFs of Ca-O, P-O and Si-O, as presented in Fig. 1. With parameters of Ca, we only investigate in the range of 5–30% mol P_2O_5, at 40% mol P_2O_5 there is no Ca. In general, we found that the distance of Ca-O, P-O, Si-O or first peaks position of graphs are almost unchanged, but the height of the peaks decreased. This tendency is similar to the results reported in [13] that the height of first peaks of P-O and Si-O RDFs declines with the rising of P_2O_5 ratio. The distances of Ca-O, P-O and Si-O are of 2.28–2.3Å, 1.56–1.58Å and 1.64–1.68Å, respectively. These calculations resemble other experimental and simulation results presented in Table 2. The graphs of RDF of P-O and Si-O have sharp peaks, it is quite consistent with the observation in [13] where the authors showed that Si-O and P-O are tight bonds and O atoms cannot easily escape the Coulombic force's effect area of P and Si ions. The first peak height of RDFs of Si-O and P-O is higher than that of RDF of Ca-O, indicating a higher concentration. Correspondingly, the coordination numbers of Si-O and P-O are more stable than those of Ca-O (Fig. 2). It shows a slight influence of the ratio of P_2O_5 on the Si-O and P-O bond of the material system CPS. We also found that there was a similarity in link distance variation in our study and some previous studies (Table 2). With different structural components, the P-O and Si-O distances have a very small change, one can see the same consequence in [14].

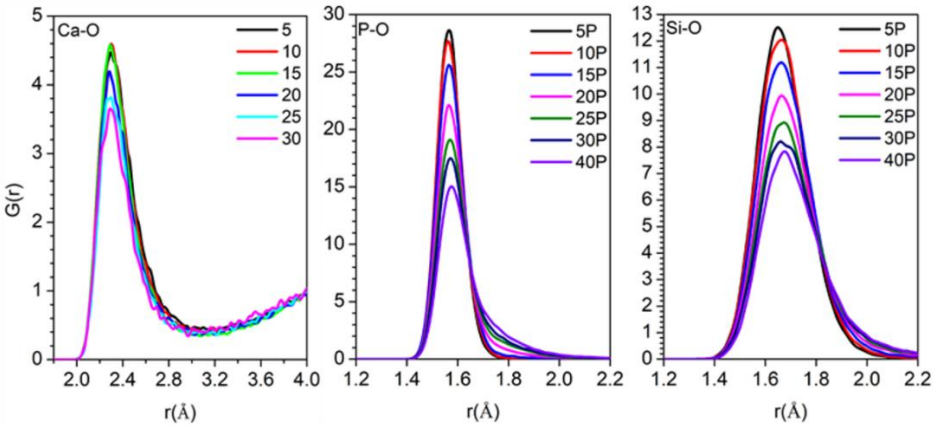

Figure 1. Radial distribution function (RDF) of Ca-O, P-O, Si-O with different P_2O_5 ratios.

Table 2. Structure characteristics of CaO-P2O5-SiO2

Ref.		d(Ca-O) (Å)	d(P-O) (Å)	d(Si-O) (Å)
This work		2.28- 2.3	1.56-1.58	1.64-1.68
[2]	0% mol P2O5	2.307 ± 0.005	-	1.610
	5% mol P2O5	2.304 ± 0.003	1.538	1.610
	10% mol P2O5	2.298 ± 0.004	1.536	1.609
	15% mol P2O5	2.306 ± 0.004	1.533	1.610
	20% mol P2O5	2.300 ± 0.002	1.526	1.611
[14]		2.25-2.32	1.55	1.63
[4]		-	1.53	1.61
[1]		2.25-2.32	1.55	1.63
[18]	S45P0	2.30/2.55±0.05	-	1.60±0.01
	S45P1	2.30/2.60±0.05	1.60±0.05	1.60±0.01
	S45P3	2.30/2.55±0.05	1.60±0.05	1.60±0.01
	S45P5	2.33/2.55±0.05	1.60±0.05	1.60±0.01

Figures 2 and 3 show the CN of Ca, P and Si. We have found that the CN of Si and P is more than 4 and surge linearly with the uptrend of P_2O_5 concentration. CN of Si goes up from 4.00 to 4.27 and P – from 4.00 to 4.49. This is similar to the conclusion in [19], CN of Si-O is almost 4 and [SiO_4] tetrahedrons have a high stability. On the other hand, the graph of CN of Ca-O has some slight shifts in the range of 5.15 and 5.36 when increasing the ratio of P_2O_5 (Fig. 2). The CN is appropriate 5 of Ca-O that has also seen in CPS system [14]. Data on specific coordination numbers are presented in Table 3.

Table 3. Coordination number of MOx (M=Ca, P, Si) with different P_2O_5 ratios

	Concentrations of P_2O_5 (% mol)						
	5	10	15	20	25	30	40
CN CaOx	5.36	5.17	5.15	5.25	5.16	5.35	-
CN POx	4.00	4.00	4.04	4.14	4.27	4.34	4.49
CN SiOx	4.01	4.02	4.06	4.11	4.19	4.24	4.27

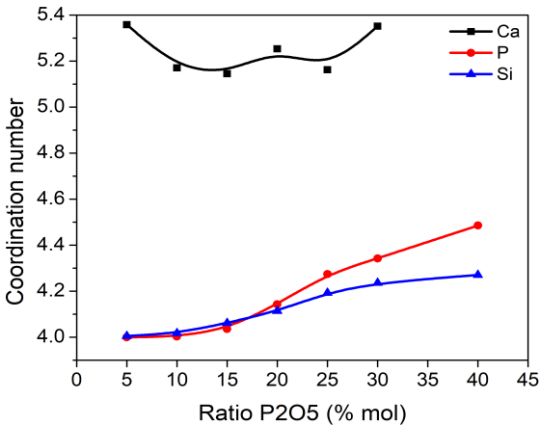

Figure 2. Coordination number of Ca, P, Si with concentrations of P_2O_5.

The instability in the CN of CaO_x can be seen in Fig. 3. CaO_x exists as many units of CaO_3-CaO_8 where CaO_5 is the majority, more than 35% (in the range of 35.99% and 41.67%). The graph of CaO_5 rises to a peak at 20% P_2O_5 and then gradually decreases. CN 4 and CN6 account for about 20-30%. CN7 is of 6.75-14.84%. The CN3 and CN8 accounts remain for a very low percentage. Because the CN is dispersed over a wide range (from 3 to 8), the graph of RDF of Ca-O has much lower first peaks than that of RDFs of Si-O and P-O.

Figure 3 shows that the Si and P coordination number distributions have quite similar shapes. In both PO_x and SiO_x, the CN4 is the majority. CN4 of SiO_x is in the range of 74.86% and 99.47% and decreases with increasing P_2O_5 ratio. These statistical data are not much different from the results reported in [4, 13, 14], namely more 80% of Si-O and more 90% of P-O are in 4 coordination; the CNs of Si-O and P-O decline slightly with as the P_2O_5 ratio soars. The CN5 and CN6 of PO_x increase with increasing P_2O_5 ratio, from 0.53% to 23.19% and from 0 to 1.94%, respectively. Similarly, the CN4 ratio in PO_x decreases linearly from 100% to 66.35%. The CN5 and CN6 concertraitions ascend continually from 0% to less than 20%. The sizable decline of the ratio of the majority coordination number (CN4) also leads to a decrease in the first peak height of the RDFs P-O and Si-O.

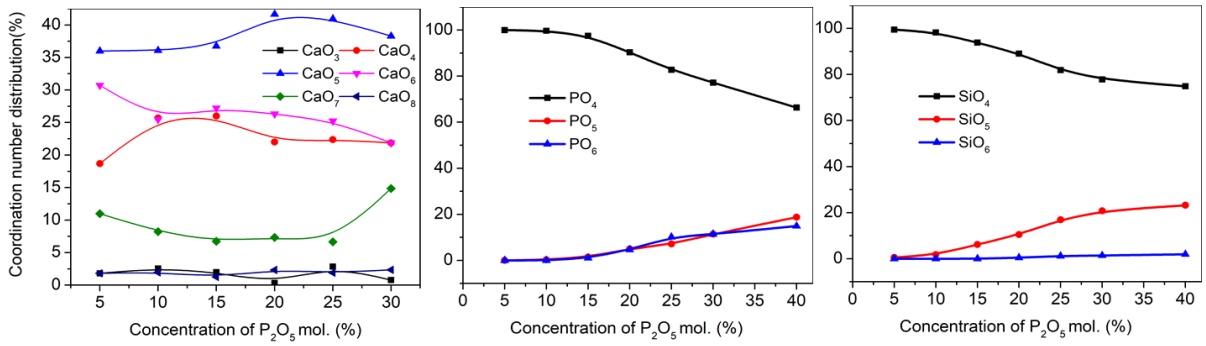

Figure 3. Coordination number distribution with different concentrations of P_2O_5.

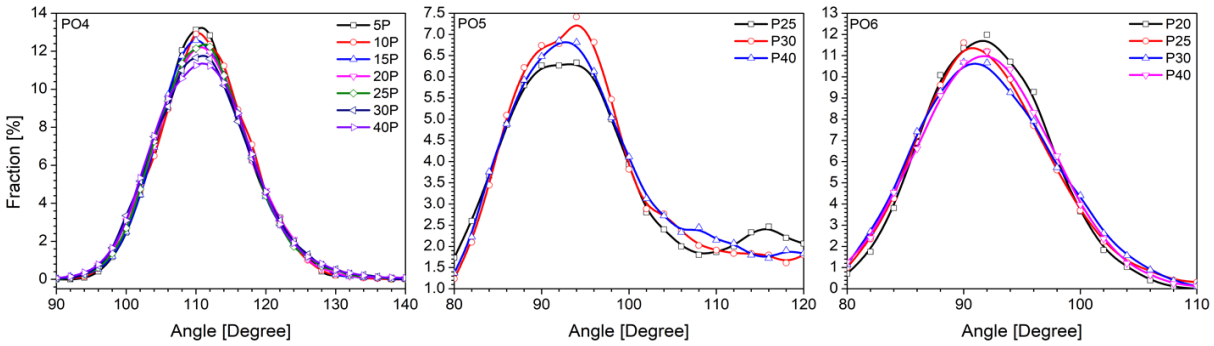

Figure 4. Bond angle distribution (BAD) of OPO in POx (x=4, 5, 6) with different P_2O_5 ratios.

The coordination number of POx exists mainly 4, the graph of the PO_4 BAD and BDD can be seen very clearly with different P_2O_5 concentration. The number of CN5 and CN6 is small and exists with the high P_2O_5 ratio, so we consider only the BADs and BDDs of PO_5 and PO_6 with high P_2O_5 ratio, see Fig. 4 and Fig. 5. Figure 4 shows that the angle OPO in PO_4 is of mainly 110^0-112^0, compared approximately with the result of Fan et al., [14] showing that OPO angle is of 109^0. The angle value is

almost constant, but the peak height of the BAD drops gradually with increasing concentration of P_2O_5. This decreasing tendency emerges because of the ratio of [PO_4] tetragedrons ratio declines with increasing P_2O_5 ratio. Correspondingly, the P-O bond length is 1.54–1.56Å and remains steadily with rising ratio of P_2O_5 (Fig. 5). With P_2O_5 25–40% mol, the OPO angle in PO_5 is of 92^0–94^0 and the P-O distance is of 1.6Å. With a high P_2O_5 ratio (20–40% mol), the OPO angle in PO_6 is of 90^0–92^0 and the corresponding P-O bond is 1.7Å. As can be seen, the microstructural parameters related to PO_x are less affected by the concentration of P_2O_5.

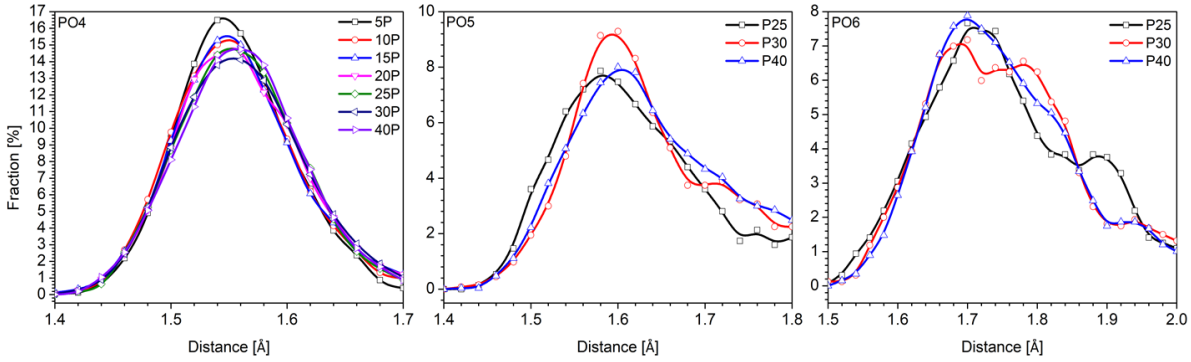

Figure 5. Bond distance distribution (BDD) P-O in POx (x=4, 5) with different P_2O_5 ratios.

Figures 6 and 7 show the BADs and BDDs of the units of SiOx (x = 4, 5). Because of the concentration of number coordination of SiO_x, SiO_4 is the predominant form of existence and SiO_5 occupies a small proportion when the ratio of P_2O_5 is high, we just investigate BADs and BDDs with corresponding conditions. The OSiO angle in SiO_4 is of 108^0–112^0 and Si-O distance is of 1.64–1.66Å. The OSiO angle in SiO_5 is appropriate 90^0 and Si-O bond length is in the range of 1.76 and 1.78Å. In a previous study [4], Tilocca et.al also has similar results that the SiO_2-Na_2O-CaO-P_2O_5 system in 3,000K, OSiO angle in SiO_4 and SiO_5 is 108^0 and 90^0, respectively. In other work [19], for the CaO-SiO_2-TiO_2 system, OSiO angle in SiO_4 is of 105^0–110^0. We compared the similarity of the data measured of tetrahedrally sillicon sample of optical quality fused quartz supplied by Engelhard Industries Inc. under the trade name Amersil in the Mozzi and Warren [20], that Si-O bond length is of 1.62Å and OSiO angle is of 109.5^0. We have seen that the SiO_x structures in bioglass systems are stable with the shifts of the networks modifiers, networks formers, networks breaker. The change of P_2O_5 concentration did not have much impact on the microstructural parameters of the SiO_x units.

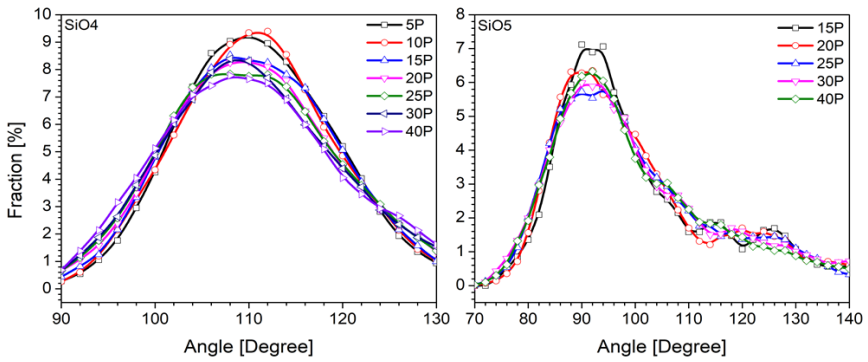

Figure 6. BAD of OSiO in SiOx (x=4, 5) with different P_2O_5 ratios.

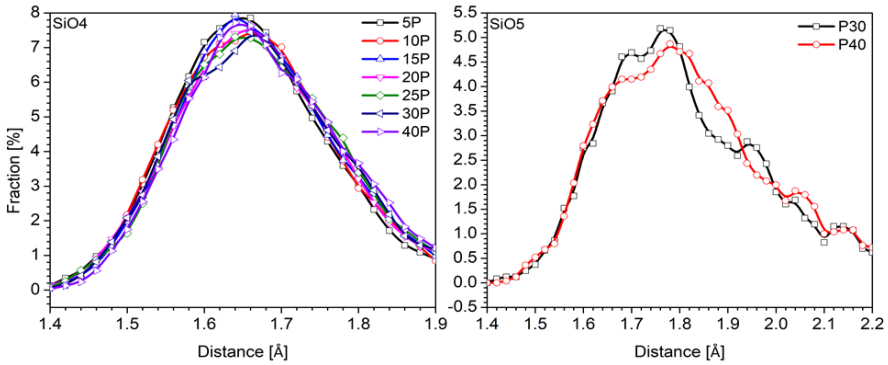

Figure 7. BDD Si-O in SiOx (x=4, 5) with different P_2O_5 ratios.

OTO angle in TO_4 units is of 110^0, In TO_5 is of 90^0–94^0, in TO_6 is of 90^0–92^0, see Fig. 8. These values are similar to those of PO_x and SiO_x and quite stable when changing the concentration of P_2O_5. The figure has the main peak at 110^0, a shoulder at 94^0 and a small peak at 174^0. The main peak corresponds to OTO angle with CN = 4, and a shoulder corresponds to OTO angle in TO_5.

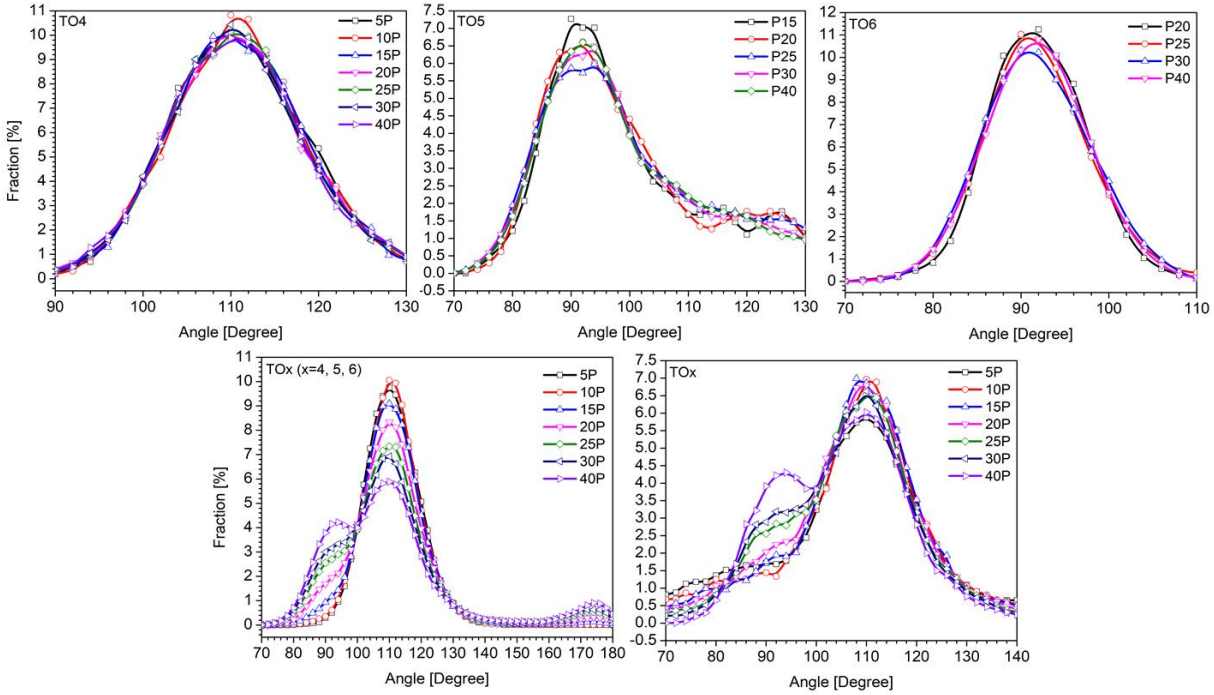

Figure 8. BAD of TOx with different P_2O_5 ratio.

3.2. Intermediate Range Order (IRO)

RDF of Ca-P shows that Ca-P bond length is in the range of 3.64Å and 3.7Å, the peaks height decreases with increasing P_2O_5 ratio. Distance of Ca-Si increases from 3.62Å to 3.68Å, the height of the peaks decreases when increasing P_2O_5 ratio. The P-P bond length is of 3.33Å –3.28Å, P-Si bond length

is 3.24A–3.28Å, Si-Si bond length is 3.26A–3.2Å. The distance of O-O is of 2.52Å–2.66Å, the distance decreases and the height peak increases with P_2O_5 ratio.

The variation of OM_y ratio is presented in Fig. 9 and Table 4. The OM_2 has the highest percentage. The OM_2 ratio increases from 52.42% to 78.08%, reach the highest point at 20% mol P_2O_5, then decreases to 47.31%. The OM_3 accounts for the second largest percentage. The OM_3 is 35.3% as the ratio of P_2O_5 is 5% mol, then hit a low of 17.03% (at 20% mol P_2O_5), then increases to appropriately 30%. The OM_4 accounts for the lowest percentage, declines from 11.52% to 1.47% (at 20% mol P_2O_5), then go up to 14.14%. We can see that the analogous tendency of the fluctuation of OM_4 and OM_3 concentration. It shows that the degree of agglomeration of the material system increases when the ratio of P_2O_5 increases.

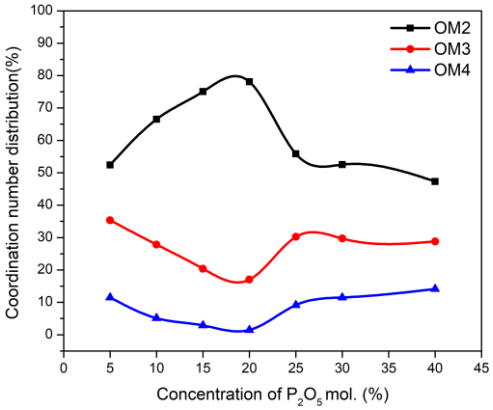

Figure 9. Coordination number distribution of OMy units with different P_2O_5 ratios.

Table 4. OMy units with different P_2O_5 concentration

OMy		Concentration of P2O5 (%mol)						
		5	**10**	**15**	**20**	**25**	**30**	**40**
OM1	Ca0P1Si0	3	9	50	100	83	117	180
	Ca0P0Si1	0	2	4	21	9	7	12
	SUM	**3**	**11**	**54**	**121**	**92**	**124**	**192**
OM2	Ca1P1Si0	126	293	396	327	230	170	0
	Ca1P0Si1	119	112	87	82	58	40	0
	Ca0P1Si1	199	486	922	1248	899	937	1086
	Ca0P2Si0	1	6	24	143	107	156	227
	Ca0P0Si2	1348	1365	1213	1011	738	609	504
	SUM	**1793**	**2262**	**2642**	**2811**	**2032**	**1912**	**1817**
OM3	Ca1P1Si1	30	54	59	78	146	114	0
	Ca0P1Si2	1	3	16	25	481	567	659
	Ca0P2Si1	0	0	4	11	158	194	386
	Ca1P2Si0	0	1	4	5	3	4	0
	Ca2P1Si0	299	411	362	345	90	54	0
	Ca1P0Si2	300	133	75	62	78	52	0
	Ca2P0Si1	578	343	197	86	75	24	0
	Ca0P0Si3	0	2	0	1	69	72	61
	SUM	**1208**	**947**	**717**	**613**	**1100**	**1081**	**1106**

OM4	Ca0P1Si3	0	0	0	1	126	183	245
	Ca0P2Si2	0	0	0	0	86	137	295
	Ca3P1Si0	85	84	57	39	4	1	0
	Ca1P0Si3	0	0	0	0	8	4	0
	Ca3P0Si1	269	80	39	11	7	3	0
	Ca2P0Si2	31	6	0	0	6	3	0
	Ca1P1Si2	0	0	0	0	36	42	0
	Ca1P2Si1	0	0	0	1	6	10	0
	Ca2P1Si1	5	4	6	1	54	31	0
	SUM	**390**	**174**	**102**	**53**	**333**	**414**	**540**
OM5	Ca0P1Si4	0	0	0	0	17	20	42
	Ca4P1Si0	9	2	4	1	0	0	0
	Ca4P0Si1	9	4	0	0	0	0	0
	Ca0P2Si3	0	0	0	0	33	55	112
	SUM	**18**	**6**	**4**	**1**	**50**	**75**	**154**

OM_2 exists mainly in the form of O-2Si and O-(P, Si). O-2Si ratio goes down from 75.18% to 27.74% and O-(P, Si) goes up from 11.1% to 59.77% with increasing the P_2O_5 ratio. O-(2P), O-(1Ca, 1Si), O-(1Ca, 1P) account for small percentages, less than 20%, the rates have some slight shifts when concentration of P_2O_5 changed. The OM_3 is in O-(xCa, yP, zSi) forms. O-(1P, 2Si) increases continually from 0.08% to 59.58%. O-(2Ca, 1Si) decreases linerly from 47.85% to 0%. O-(2Ca, 1P) surges dramatically from 24.75% to the peak at 56.28% (20% mol P2O5), then decrease to 0%. O-(1Ca, 2Si) and O-(1P, 2Si) is lower 40%. The ratio of OM_4 units also varies greatly with the concentration of P_2O_5. O-(1P, 3Si) and O-(2P, 2Si) increase linerly from 0 to 45.37% and 45.37%, respectively. O-(3Ca, 1Si) shrinks consistently from 68.97% to 0%. O-(3Ca, 1P) increases from 21.7% to 73.58% (at 20% mol P_2O_5) then falls to 0% (see Fig. 10). We analys that the concentration of P_2O_5 has a significant impact on fraction of OM_y units and 20%mol P_2O_5 causes a huge variation.

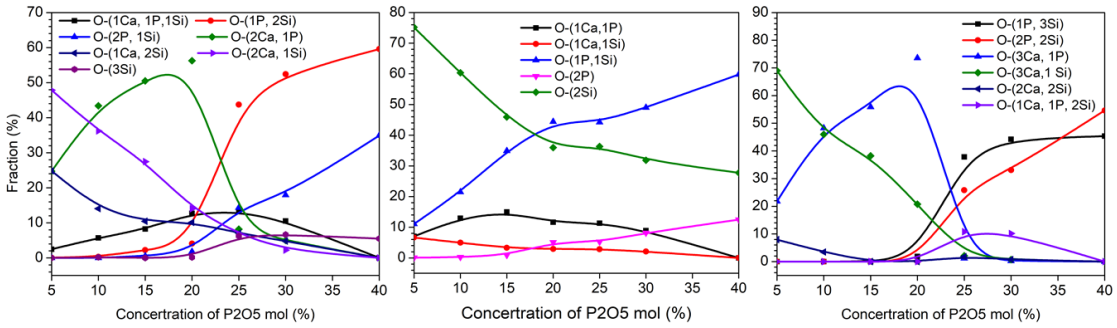

Figure 10: Fraction of OMy (y=2, 3, 4) units with different P_2O_5 ratios.

Figure 11 shows the fraction of BO and NBO changing with the concentration of P_2O_5. The percentage of BO grows steadily when the concentration of P_2O_5 increases, from 55.75% with 5% mol P_2O_5 to 94.86%. The NBO ratio declines significantly from 44.25% to 5.13%. The fraction of free oxygen (FO) is almost non-existent. It shows the polymerization of the CPS system increases remarkably.

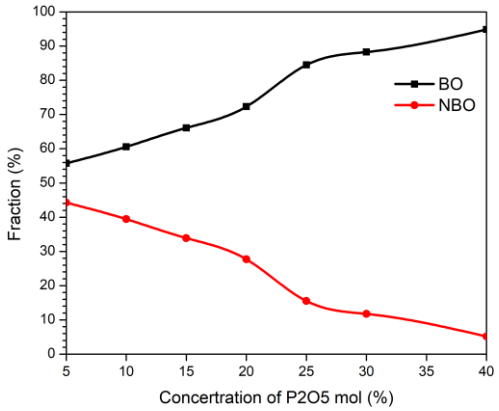

Figure 11. Fraction of BO and NBO with different P_2O_5 ratios.

BO units are mainly P-O-Si and Si-O-Si bonds form, a small part is P-O-P bond. When increasing P_2O_5 concentration, P-O-P bond fraction increases from 0 to 18.44%. In the same P_2O_5 concentration range, Si-O-Si bond fraction falls from 87.48% to lowest 42.5% (20% mol P_2O_5), then rises to around 50%. P-O-Si bond ratio increases from 12.46% to the peak at 51.31% (20% mol P_2O_5), then declines to 32.66%. We found that in the range of 0–20% mol P_2O_5, the upward and downward tendencys of type of BO are similar to the one reported in [13]. The oxygen bonding with only Si atoms has a high ratio with low P_2O_5 ratio, then drops remarkably to 15.21% when increasing the P_2O_5 ratio. On the contrary, the fraction of BO with only (P, Si) soars significantly from 12.88% to 74.1%. The Oxygen bonding with only Si has a small percentage and increases with P_2O_5 concentration (from 0.26 to 10.68%). The NBO units exist mainly as O-(2Ca, 1P), O-(2Ca, 1Si), O-(1P), O-(1Ca, 1P), etc. The O-(1P) ratio increases remarkably from 0.2 to 100% when increasing from 0-40% mol P_2O_5. The other types of NBOs account for less than 50% and fluctuate a lot when the ratio of P_2O_5 changes. The proportions of the types of bonding are shown in Fig. 12.

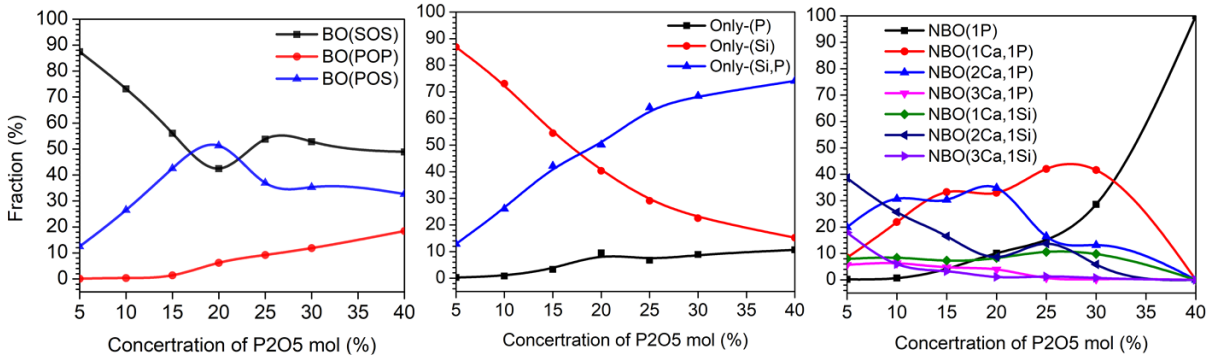

Figure 12. The fraction of the types of BO, NBO, Oxygen bonding only (P, Si).

The [SiO4] cluster distribution is shown in Table 5. We find that with 5%mol P_2O_5, the size of the atomic cluster is very large, and the material system is almost clustered into a single cluster with 3,947 atoms. In addition, there are some small clusters with only 5 or 9 atoms. As the concentration of P_2O_5 increased, the largest cluster size gradually decreased, and the material system CPS appeared in many smaller clusters. The largest cluster size with 40% mol P_2O_5 is 123 atoms, in addition, there are many clusters with only a few dozen atoms. With 5% mol P_2O_5 there are less than 10 clusters of 5 atoms,

increasing to 124 clusters when reaching 40% mol P_2O_5. This shows that the atomic cluster distribution is greatly influenced by the concentration of P_2O_5.

Table 5. The SiO4 clusters distribution (Nc is the number of clusters, Na is the number of atoms in this cluster)

5P		10P		15P		20P		25P		30P		40P	
Nc	Na	Nc	Na	Nc	Na	Nc	Na	Nc	Na	Nc	Na	Nc	Na
9	5	7	5	20	5	31	5	68	5	85	5	124	5
3	9	1	9	4	9	10	9	22	9	26	9	39	9
1	3,947	1	3,506	1	13	4	13	9	13	12	13	12	13
				1	17	2	17	5	17	5	17	8	17
				1	3,196	2	25	4	21	4	21	7	21
						1	2,649	1	24	3	25	2	25
								2	25	4	29	3	29
								3	29	1	33	1	32
								2	33	1	36	1	33
								3	45	5	37	1	37
								1	65	1	40	1	41
								1	81	1	43	1	45
								1	148	1	53	1	48
								1	202	1	57	2	49
								1	331	1	63	1	53
								1	707	1	65	2	56
										1	136	1	57
										1	602	1	69
												1	123

Contrary to the distribution of [SiO4] clusters, the [PO4] clusters increase in size with increasing P_2O_5 concentration. Of course, as the concentration of P_2O_5 increases, the number of [PO4] atoms also increases and most of the clusters have only 5 atoms, but at high concentrations of P_2O_5, clusters of more than 20 atoms appear (see Table 6). We find that with upward trend of P_2O_5 5% mol, there are more small clusters of tetrahedron unit of P and Si and the number atoms of biggest clusters declines.

Table 6. The PO4 clusters distribution

5P		10P		15P		20P		25P		30P		40P	
Nc	Na	Nc	Na	Nc	Na	Nc	Na	Nc	Na	Nc	Na	Nc	Na
186	5	1	4	440	5	455	5	397	5	412	5	390	5
1	9	325	5	14	9	43	9	69	9	74	9	79	9
		7	9	1	13	1	13	11	13	15	13	19	13
								3	17	1	17	7	17
										1	21	3	21
												1	24
												1	25

4. Conclusion

- The bond distances of Ca-O, P-O and Si-O are of 2.28Å–2.3Å, 1.56Å–1.58Å and 1.64Å–1.68Å, respectively. The bond lengths are less affected by the P_2O_5 concentration. The height of the first peaks of PRDs decreases as increasing P_2O_5 ratio.

- The CN of Ca-O is in the range of 5.15 and 5.35, of PO_x is 4.00-4.29, and that of SiO_x is 4.00-4.27. Si and P mainly exist in the form of CN=4. The CNs of SiO_x and PO_x increases with the increase of P_2O_5 volume.

- The distances of Si-O and P-O and OPO, OSiO angles of in SiO_x, PO_x have small fluctuations with the change of P_2O_5 concentration. The data of bond angle and distance distribution show these values have variation of about 0^0–2^0 and 0–2Å, respectively.

- The ratio of OM_y units are dependent on the P_2O_5 concentration. OM_y exist mainly as MO_2, OM_3, OM_4. The ratios of these units reach their maximum and minimum at the 20% mol P_2O_5.

- The polymerization of the CPS system increases as the P_2O_5 ratio increases. The fraction of BO increases, whereas fraction of NBO decreases. The data of BOs such as P-O-P, Si-O-Si, P-O-Si reach their maximum and minimum at the 20% mol P_2O_5.

- The structure of the material system changes a lot when increasing P_2O_5 concentration. The atom clusters [SiO4] are distributed oppositely, at low P_2O_5 concentration, almost all the atoms gather into a very large cluster, while at high P_2O_5 concentration, the atomic clusters are numerous but small in size. On the contrary, [PO4] clusters tend to increase in size with higher concentration of P_2O_5.

References

[1] L. L. Hench, The story of Bioglass, J. Mater. Sci. Mater. Med., Vol. 17, No. 11, 2006, pp. 967-978, https//doi.org/10.1007/s10856-006-0432-z.

[2] Q. Chen, Bioglass-derived Glass-ceramic Scaffolds for Bone Tissue Engineering, 2006.

[3] L. Hupa, Composition-property Relations of Bioactive Silicate Glasses, Bioact. Glas., 2018, pp. 1-35, https//doi.org/10.1016/b978-0-08-100936-9.00001-0.

[4] A. Tilocca, Structure and Dynamics of Bioactive Phosphosilicate Glasses and Melts from Ab Initio Molecular Dynamics Simulations, Phys. Rev. B - Condens. Matter Mater. Phys., Vol. 76, No. 22, 2007, pp. 1-13, https//doi.org/10.1103/PhysRevB.76.224202.

[5] N. V. Hong, N. T. T. Ha, P. K. Hung, T. Iitaka, Pressure-induced Structural Change of Cao–Al2O3–Sio2 Melt: Insight from Molecular Dynamics Simulation, Mater. Chem. Phys., vol. 236, No. April, 2019, pp. 121839, https//doi.org/10.1016/j.matchemphys.2019.121839.

[6] K. Zheng, Z. Zhang, F. Yang, S. Sridhar, Molecular Dynamics Study of the Structural Properties of Calcium Aluminosilicate Slags with Varying Al_2O_3/SiO_2 Ratios, Vol. 52, No. 3, 2012, pp. 342-349.

[7] M. Fábián et al., Network Structure and Thermal Properties of Bioactive (SiO_2–CaO–Na_2O–P_2O_5) Glasses, J. Mater. Sci., Vol. 55, No. 6, 2020, pp. 2303-2320, https//doi.org/10.1007/s10853-019-04206-z.

[8] S. Bose, S. Tarafder, Calcium phosphate Ceramic Systems in Growth Factor and Drug Delivery for Bone Tissue Engineering: A Review, Acta Biomater., Vol. 8, No. 4, 2012, pp. 1401-1421, https//doi.org/ 10.1016/j.actbio.2011.11.017.

[9] S. N. F. S. Adam, F. Zainuddin, A. F. Osman, Effect of Varying Phosphate Content on the Structure and Properties of Sol-gel Derived SiO_2-CaO-P_2O_5 Bio-glass, J. Phys. Conf. Ser., Vol. 2080, No. 1, 2021, https//doi.org/10.1088/1742-6596/2080/1/012018.

[10] P. Kiran, V. Ramakrishna, M. Trebbin, N. K. Udayashankar, H. D. Shashikala, Effective role of CaO/P_2O_5 Ratio on SiO_2-CaO-P_2O_5 Glass System, J. Adv. Res., Vol. 8, No. 3, 2017, pp. 279-288, https//doi.org/10.1016/j.jare.2017.02.001.

[11] C. C. Lin, S. F. Chen, K. S. Leung, P. Shen, Effects of CaO/P_2O_5 Ratio on the Structure and Elastic Properties of SiO_2-CaO-Na_2O-P_2O_5 Bioglasses, J. Mater. Sci. Mater. Med., Vol. 23, No. 2, 2012, pp. 245-258, https//doi.org/10.1007/s10856-011-4504-3.

[12] G. Malavasi, L. Menabue, M. C. Menziani, A. Pedone, A. J. Salinas, M. V. Regí, New Insights Into the Bioactivity of SiO_2-CaO and SiO_2-CaO-P_2O_5 sol-gel Glasses by Molecular Dynamics Simulations, J. Sol-Gel Sci. Technol., Vol. 67, No. 1, 2013, pp. 208-219, https//doi.org/10.1007/s10971-011-2453-4.

[13] J. Diao, G. Fan, X. Liu, B. Xie, Computer Simulation of Anionic Structures of Molten CaO-SiO_2-P_2O_5 System, Metall. Mater. Trans. B Process Metall. Mater. Process. Sci., Vol. 45, No. 5, 2014, pp. 1942-1947, https//doi.org/10.1007/s11663-014-0092-1.

[14] G. Fan, J. Diao, L. Jiang, Z. Zhang, B. Xie, Molecular Dynamics Analysis of the Microstructure of the Cao-P_2O_5-SiO_2 Slag System with Varying P_2O_5/SiO_2 Ratios, Mater. Trans., Vol. 56, No. 5, 2015, pp. 655-660, https//doi.org/10.2320/matertrans.M2014363.

[15] A. J. Salinas, A. I. Martin, M. V. Regí, Bioactivity of three CaO-P_2O_5-SiO_2 sol-gel Glasses, J. Biomed. Mater. Res., Vol. 61, No. 4, 2002, pp. 524-532, https//doi.org/10.1002/jbm.10229.

[16] M. Laczka, K. C. Kowalska, A. L. Osyczka, M. Tworzydlo, B. Turyna, Gel-derived Materials of A Cao-P_2O_5-SiO_2 System Modified by Boron, Sodium, Magnesium, Aluminum, and Fluorine Compounds, J. Biomed. Mater. Res., Vol. 52, No. 4, 2000, pp. 601-612, https//doi.org/10.1002/1097-4636(20001215)52:4<601::AID-JBM4>3.0.CO;2-I.

[17] M. Łączka, K. C. Kowalska, K. Kulgawczyk, M. Klisch, W. Mozgawa, Structural Examinations of Gel-Derived Materials of the CaO-P_2O_5-SiO_2 System, J. Mol. Struct., Vol. 511-512, 1999, pp. 223-231, https//doi.org/10.1016/S0022-2860(99)00163-5.

[18] J. Huang, Design and Development of Ceramics and Glasses, Biol. Eng. Stem Cell Niches, 2017, pp. 315-329, https//doi.org/10.1016/B978-0-12-802734-9.00020-2.

[19] S. Zhang, X. Zhang, C. Bai, L. Wen, X. Lv, Effect of TiO_2 content on the structure of CaO-SiO_2-TiO_2 System by Molecular Dynamics Simulation, ISIJ Int., Vol. 53, No. 7, 2013, pp. 1131-1137, https//doi.org/10.2355/isijinternational.53.1131.

[20] R. L. Mozzi, B. Warren, Structure of Vitreous Silica, J. Appl. Crystallogr., Vol. 2, No. pt4, 1969, pp. 164-172, https//doi.org/10.1107/S0021889869006868.